



Comparative Evaluation of LMR-NCM and NCA Cathode Active Materials in Multilayer Lithium-Ion Pouch Cells: Part II. Rate Capability, Long-Term Stability, and Thermal Behavior

Ludwig Kraft,^{1,*} Tanja Zünd,^{2,*} David Schreiner,³ Rebecca Wilhelm,^{2,*} Florian J. Günter,³ Gunther Reinhart,³ Hubert A. Gasteiger,^{2,**} and Andreas Jossen¹

¹Institute for Electrical Energy Storage Technology, Technical University of Munich, D-80333 Munich, Germany

²Chair of Technical Electrochemistry, Technical University of Munich, D-85748 Garching, Germany

³Institute for Machine Tools and Industrial Management, Technical University of Munich, D-85748 Garching, Germany

A lithium- and manganese-rich layered transition metal oxide-based cathode active material (LMR-NCM) with a reversible capacity of 250 mAh g⁻¹ vs graphite is compared to an established NCA/graphite combination in multilayer lithium-ion pouch cells with a capacity of 5.5 Ah at a 1C discharge rate. The production of the cells, the electrode characterization as well as the formation is described in Part I of this study. In Part II, the two cell types are evaluated for their rate capability and their long-term stability. The specific capacity of the LMR-NCM pouch cells is ≈30% higher in comparison to the NCA pouch cells. However, due to the lower mean discharge voltage of LMR-NCM, the energy density on the cell level is only 11% higher. At higher discharge currents, a pronounced heat generation of the LMR-NCM pouch cells was observed, which is ascribed to the LMR-NCM voltage hysteresis and is only detectable in large-format cells. The cycling stability of the LMR-NCM cells is somewhat inferior due to their faster capacity and voltage fading, likely also related to electrolyte oxidation. This results in a lower energy density on the cell level after 210 cycles compared to the NCA pouch cells.

© 2021 The Author(s). Published on behalf of The Electrochemical Society by IOP Publishing Limited. This is an open access article distributed under the terms of the Creative Commons Attribution 4.0 License (CC BY, <http://creativecommons.org/licenses/by/4.0/>), which permits unrestricted reuse of the work in any medium, provided the original work is properly cited. [DOI: 10.1149/1945-7111/abe566]



Manuscript submitted January 14, 2021; revised manuscript received February 11, 2021. Published February 23, 2021.

The demand for lithium-ion batteries with a higher capacity and energy density is rising, especially driven by mobile applications like electric vehicles (EVs).^{1–4} As a consequence, the specific capacity of the active materials must increase. State-of-the-art cathode active materials (CAMs) are lithium-nickel-cobalt-manganese-oxides (NCMs) or lithium-nickel-cobalt-aluminum-oxides (NCAs). The capacity of NCMs can be increased by a higher Ni content, e.g., from NCM-111 with 150 mAh g⁻¹ up to 200 mAh g⁻¹ for NCM-811 for comparable upper cutoff voltages.^{1,2,5} The Ni-rich NCA materials exhibit a similar specific capacity of around 200 mAh g⁻¹.^{6,7} A promising not yet commercialized CAM that offers a higher capacity is Li- and Mn-rich NCM (LMR-NCM) with a reversible capacity of around 250 mAh g⁻¹.^{8–12}

Material costs account for 45%–75% of the total manufacturing costs on the cell level, and the CAMs have the biggest share of the material costs with 39%–54%.^{13–16} This makes Mn-rich materials more cost effective compared to Ni-rich materials. In February 2021, the price of the commodity Ni (21 USD kg⁻¹)¹⁷ was an order of magnitude higher than that of Mn (2 USD kg⁻¹).¹⁸ While currently used NCA and NCM CAMs still contain Co, ongoing research aims toward reducing or eliminating Co.^{19–21} Similarly, it has also been shown that Co can be eliminated from LMR-NCM CAMs.²² Based on the stoichiometry of the two CAMs that are investigated in our work, up to 34% can be saved in raw material costs comparing a LMR-NCM (Li_{1.14}Ni_{0.26}Co_{0.14}Mn_{0.60}O₂) to an NCA (LiNi_{0.81}Co_{0.15}Al_{0.04}O₂) with commodity prices of Co (45 USD kg⁻¹),²³ Li (10 USD kg⁻¹),²⁴ and Al (2 USD kg⁻¹).²⁵ Therefore, the high specific capacity combined with the lower material costs render LMR-NCM to a promising CAM for future lithium-ion batteries.^{4,11,26,27}

There is a wide variety of lithium-ion cells exhibiting different cell formats, designs, and materials. Reported energy densities of various cells and cell formats range from 83 Wh kg⁻¹ for high power cells to 267 Wh kg⁻¹ for high energy cells.^{28–31} The energy density on the cell level can be enhanced by thicker and less porous electrodes, by

electrode compositions with a higher active material share, or by the use of active materials with a higher specific capacity, while reducing the share of passive parts like separators, current collectors, tab connectors, or the housing.^{1,32} Up-to-date, high energy cells that reach >250 Wh kg⁻¹ often use a Ni-rich CAM, either NCM-811 or NCA, and a graphite anode that contains a small amount of silicon.^{29–31,33} Ding et al.³⁰ reported energy densities of cylindrical cells used by Tesla in EVs of 236 Wh kg⁻¹ for an NCA/graphite cell and 260 Wh kg⁻¹ for an NCA/silicon-graphite cell.

In this work, a LMR-NCM material is evaluated and compared to a commercially available NCA material that serves as a benchmark. Based on our scale-up experiments with laboratory-scale coin cells with LMR-NCM, this CAM was used to design multilayer pouch cells, which were produced on the pilot scale production line at the Technical University of Munich,³⁴ as described in Part I of this study.³⁵ To appropriately assess the performance of the LMR-NCM pouch cells, NCA pouch cells with the same electrode and cell configuration were produced on the same line. The cells were standardized by adjusting the loading of the electrode sheets, delivering an areal capacity of 2.3 mAh cm⁻² or a total capacity of 5.5 Ah at a 1C discharge rate. For both cell types, graphite was used as anode material. For simplicity, the LMR-NCM/graphite and NCA/graphite pouch cells will further on be referred to as LMR-NCM and NCA pouch cells, respectively.

The production of the cells, the electrode characterization, as well as their formation is described in Part I of this study.³⁵ In Part II, the characteristics of both cell types were evaluated by discharge rate capability tests and by an aging study, in which we compare their capacity, mean discharge voltage, and energy density fading, their internal resistance buildup, as well as their self-heating at high discharge rates. While previous publications on LMR-NCM were carried out with small-scale laboratory cells (e.g., coin cells), stating energy densities up to 1000 Wh kg⁻¹ at the material level,^{11,12,26} to the best of our knowledge, there is no published research on large-format LMR-NCM cells that would allow a rigorous assessment of the energy densities achieved on the cell level. Especially the evaluation of self-heating effects at high C-rates and gassing effects during formation and extended aging is only feasible with large-format cells, so that the here presented study with large-format multilayer pouch cells will provide new insights with regards to these aspects.

*These authors contributed equally to this work.

*Electrochemical Society Student Member.

**Electrochemical Society Fellow.

^zE-mail: ludwig.kraft@tum.de

Experimental

The large-format multilayer pouch cells were produced on the semi-automatic manufacturing pilot line at the Technical University of Munich.³⁴ To compare the performance of the two CAMs, both pouch cell types were designed to have a similar areal capacity of 2.3 mAh cm⁻² at a 1C discharge, amounting to a total capacity of around 5.5 Ah at 1C. A target capacity of 5.5 Ah at 1C results in an energy of 17.6 Wh for the LMR-NCM and 19.8 Wh for the NCA pouch cells (based on averaged discharge voltages at 1C of 3.2 V for the LMR-NCM and 3.6 V for the NCA cells). The here used multilayer pouch cell design was based on small-scale laboratory coin cell measurements that were conducted in Part I of this study.³⁵ Details on the electrode production as well as the pouch cell assembly and formation are also provided in Part I of this study.³⁵

Electrode specifications.—In this study, a LMR-NCM CAM with a stoichiometry of Li_{1.14}[Ni_{0.26}Co_{0.14}Mn_{0.60}]_{0.86}O₂ (BASF, Germany), which can as well be written as 0.33 Li₂MnO₃ · 0.67 LiNi_{0.38}Co_{0.21}Mn_{0.41}O₂ and was also investigated by Teuffl et al.,³⁶ and an NCA with a stoichiometry of LiNi_{0.81}Co_{0.15}Al_{0.04}O₂ (BASF, Germany) were used. The cathodes consisted of 92.5 wt% CAM (LMR-NCM or NCA), 4 wt% conductive carbon (Super-C65, Timcal, Switzerland), 3.5 wt% polyvinylidene-fluoride binder (PVdF, Solef 5130, Solvay, Belgium), and were coated double-sided on a 15 μm aluminum substrate foil (1055 A, Korff, Switzerland). The CAM loading was set to 11.7 mg cm⁻² (≡2.9 mAh cm⁻² at C/10, based on a nominal capacity of 250 mAh g⁻¹_{CAM}) and 13.0 mg cm⁻² (≡2.6 mAh cm⁻² at C/10, based on a nominal capacity of 200 mAh g⁻¹_{CAM}) for the LMR-NCM and NCA electrode sheets, respectively. The nominal capacities of both CAMs relate to LMR-NCM/Li cells in a voltage range of 2.0–4.7 V (250 mAh g⁻¹_{CAM}) and NCA/Li cells in a voltage range of 3.0–4.5 V (200 mAh g⁻¹_{CAM}), and were used for the calculation of the nominal cell capacities as stated in Table I. The cathodes were calendered to an electrode coating porosity of 42%.

The anodes consisted of 97 wt% graphite (SGL Carbon, Germany), 1.5 wt% carboxymethyl cellulose binder (CMC Sunrose MAC200, NPI, Japan), 1.5 wt% styrene-butadiene rubber binder (SBR, Zeon, Japan), and were coated on a 11 μm copper substrate foil (Cu-PHC, hard rolled blank, with a nominal thickness of 12 μm Schlenk, Germany). The graphite electrode loadings were set to 9.5 mg cm⁻² (≡3.4 mAh cm⁻² at C/10, based on a nominal capacity of 355 mAh g⁻¹_{graphite}) for LMR-NCM and 10.2 mg cm⁻² (≡3.6 mAh cm⁻² at C/10, based on a nominal capacity of 355 mAh g⁻¹_{graphite}) for NCA based pouch cells. The anodes were calendered to an electrode coating porosity of 30%. The resulting areal capacity ratios of negative/positive electrode (N/P ratio) were 1.17 for the LMR-NCM and 1.38 for the NCA pouch cells.

Pouch cell assembly.—Both cell types contained 16 double-coated cathodes and 17 double-coated anodes. The electrodes were alternately stacked with a z-folded monolayer polypropylene (PP) separator (Celgard 2500, France) with a thickness of 25 μm. An FEC:DEC based electrolyte (1 M LiPF₆ in a 12:64:24 (by volume) mixture of FEC:DEC:co-solvent and 2 wt% of a proprietary additive, BASF, Germany) was used for the LMR-NCM cells, while an

EC:DEC based electrolyte (1 M LiPF₆ in a 3:7 (by weight) mixture of EC:DEC and 2 wt% vinylene carbonate (VC), BASF, Germany) was used for the NCA cells. The proprietary additive improves full-cell cycle stability and has a similar effect as the one described in Ref. 37.

The individual cell specifications are listed in Table I. The CAM mass was determined by weighing the electrode sheets before the assembling process, while the finally determined mass of the cell after the electrolyte filling, the degassing after formation, and the final cell sealing process includes the current collectors, the welded-on tabs, and the pouch foil. For comparison of the cells, the specific capacity used in the later studies was related to the CAM mass. The gravimetric energy density, however, was related to the total pouch cell mass. On account of an error in the production process, the loading of the graphite anodes for the NCA pouch cells was slightly too high, resulting in an N/P ratio of 1.38 instead of the originally intended N/P ratio of 1.2. Assuming a N/P ratio of 1.17 for the NCA pouch cells (as is the case with the LMR-NCM cells), the total cell mass would be reduced by ≈4.4 g (due to a reduced anode loading by 1.6 mg cm⁻² with an active material ratio of 97 wt% and a total anode area of 2687 cm²), resulting in 4% higher gravimetric energy density values. Nevertheless, the stated gravimetric energy densities were calculated with the actual cell mass of the NCA pouch cells. For the evaluation of the volumetric energy density, a volume of ≈51.6 cm³ for the LMR-NCM and ≈49.7 cm³ for the NCA pouch cells was used (based on the cell thicknesses and the length and width of the deep-drawn pocket of the pouch bag). Unless stated otherwise, the term energy density refers to the gravimetric energy density. Based on a nominal reversible capacity at C/10 of 250 mAh g⁻¹ for LMR-NCM and 200 mAh g⁻¹ for NCA, the nominal cell capacity was calculated according to the CAM mass. In all later measurements, the C-rates for the charging and discharging procedures were referred to the nominal cell capacity at C/10 of each cell, as stated in Table I. For a detailed overview of the production and formation process of the LMR-NCM pouch cells, the reader is referred to Part I of this study.³⁵

Coin cell specifications.—As a reference, experiments with both the LMR-NCM and the NCA cathodes with graphite anodes were also conducted with laboratory 2032-type coin cells. Cathodes with 14 mm diameter and anodes with 15 mm diameter were punched out from a single side coated part of the electrodes used for the pouch cells as described above, i.e., with the same areal capacities as specified above. The electrodes were dried in a glass oven (Büchi, Switzerland) under dynamic vacuum at 120 °C for 12 h. The coin cells were assembled in an argon filled glove box (O₂, H₂O < 0.1 ppm, MBraun, Germany) with a separator of 17 mm in diameter and 50 μL of electrolyte. The separator and the electrolyte for the corresponding CAMs were the same for the coin and pouch cells.

Electrochemical measurements.—*Cell formation and mounting.*—A formation procedure with a first constant current (CC) C/15 cycle including degassing steps, followed by two CC C/10 cycles was carried out. The LMR-NCM cells were charged to 4.7 V in their first formation cycle to activate the material,¹⁰ in all subsequent cycles, the upper cutoff voltage was set to 4.6 V. A more detailed description of the formation procedure is given in Part I of this study.³⁵ The LMR-NCM

Table I. Specifications of the LMR-NCM/graphite and NCA/graphite pouch cells with an identical CAM-based areal capacity of ≈2.3 mAh cm⁻² at 1C. Note that the here used pouch cells represent a subset of the pouch cells presented in Part I of this study.³⁵

Cell type	Number of cells	CAM ^{a)} mass	Cell mass ^{b)}	Nominal cell capacity ^{c)}
LMR-NCM	5	27.64 ± 0.32 g	111.6 ± 1.6 g	6.91 ± 0.08 Ah
NCA	6	31.34 ± 0.41 g	115.8 ± 2.0 g	6.27 ± 0.08 Ah

a) CAM—cathode active material. b) Determined by weighing the cells after formation, degassing, and final sealing of the cells. c) Based on the nominal specific CAM capacity at C/10 (LMR-NCM: 250 mAh g⁻¹, NCA: 200 mAh g⁻¹).

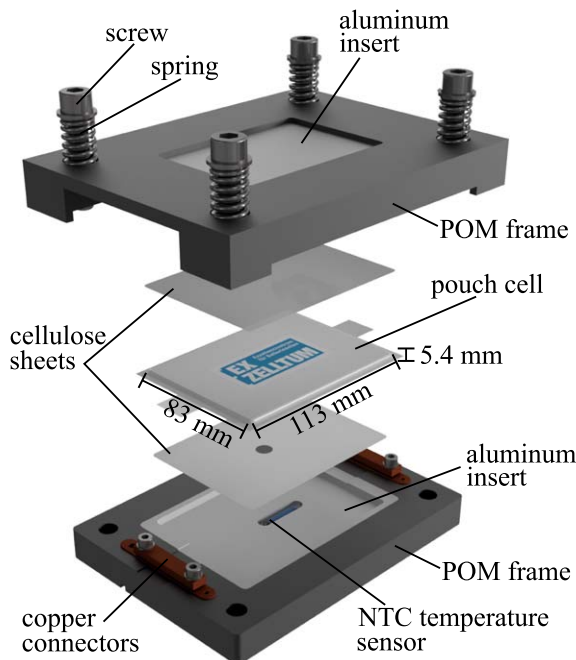


Figure 1. Schematic CAD drawing of the cell holder including the pouch cell. The 5.4 mm thickness of the depicted pouch cell represents a mean value of the thicknesses of the LMR-NCM (5.5 mm) and NCA (5.3 mm) cells.

cells were cycled between 2.0 V and 4.6 V and the NCA cells between 3.0 V and 4.3 V. Note that all C-rates are referenced to the nominal specific CAM capacity of 250 mAh g^{-1} for LMR-NCM cells and of 200 mAh g^{-1} for NCA cells.

The pouch cells were mounted in custom-built cell holders as depicted in Fig. 1. Both the bottom and top part of the cell holder consisted of a thermoplastic polyoxymethylene (POM) frame with an aluminum insert. Via the screw/spring combination a pressure of 0.2 MPa was applied to the pouch cells. Cellulose sheets (Pacopads 5500, Pacothane Technologies, USA) were put between the cell and the aluminum inserts to obtain a homogeneous compressive force across the active area. An integrated negative temperature coefficient (NTC) temperature sensor was attached to measure the temperature on the surface of the pouch cells with a precision of $\pm 1 \text{ K}$. All pouch cell measurements were performed with an XCTS battery test system (BaSyTec, Germany) in a controlled climate chamber (WT3-600/40-S, Weiss Umwelttechnik, Germany) at 25°C . The coin cells were cycled with a Maccor battery tester (series 4000, USA) in a controlled climate chamber (Binder, Germany) at 25°C . A detailed overview of all measurement procedures is listed in Table II, the tests were consecutively performed in the stated order for each of the cells.

Initial C/10 cycle and open circuit voltage curve.—After formation, the cells were charged and discharged with a CC C/10 cycle. In a subsequent CC C/10 cycle, a pause of 1 h was included after each hour, which sums up to ten 1 h pauses during the charge and ten 1 h pauses during the discharge. While pausing, the relaxation of the open circuit voltage (OCV) was measured.

Discharge rate capability test.—Next, the discharge rate capability test was carried out with CC discharging with C/10, C/5, and C/2. The preceding charging C-rate was set to the discharging C-rate. The CC charging phase was followed by a constant voltage (CV) phase until a cutoff current of C/20 was reached. For two cells of each cell type, an extended discharge rate capability test was carried out with also 1C, 2C, and 3C discharge rates, whereby the charging current in the CC phase was limited to C/2 (with a CV

phase terminated at C/20) for each discharge rate. The specific capacity was related to the mass of the corresponding CAM, whereas the energy density was related to the total cell mass as stated in Table I. The values for each cycle were averaged over all cells of the corresponding cell type and plotted with the corresponding standard deviation. If the measurement procedure only consisted of two samples, their mean value was plotted with the minimum and maximum value, indicated by the error bars.

Aging study.—In the final aging test, the cells were repeatedly cycled with a C/2 CCCV charge (with a cutoff current of C/20) and a C/2 CC discharge. Every 25 cycles, a checkup procedure was carried out. In the checkup procedure, the cells were initially charged with C/10 to a voltage of 3.7 V, which corresponds to a state-of-charge (SOC) of approximately 40% for both cell types, followed by a 1 h resting period at OCV. Then the cell resistance was determined with the direct current internal resistance (DCIR) method by applying a C/2 CC discharge pulse for 10 s and measuring the cell voltage. The resistance is calculated by Ohm's law and the total voltage drop and referenced to the cathode area (73.73 cm^2 per layer). After the DCIR test, the cells were first discharged with C/10 to their lower cutoff voltage, and then, the cell capacity was assessed by a full C/10 charge/discharge cycle. Only the four cells (2x LMR-NCM, 2x NCA) that were stressed with the extended rate capability test were additionally discharged with three 1C CC cycles in each checkup.

Results and Discussion

The comparative evaluation of the performance of the large-format multilayer LMR-NCM and NCA pouch cells is divided into two parts: the rate capability behavior, and the aging behavior of the cells in the long-term cycling study.

Rate capability behavior.—The results of the discharge rate capability test, depicting the C-rate dependence of the specific CAM capacity, the charge averaged mean cell discharge voltage, and the gravimetric cell energy density are displayed in Fig. 2; the corresponding values normalized to those at C/10 are stated in Table III.

For low C-rates, i.e., C/10 and C/5, the discharge capacity stayed almost constant for both materials, and the LMR-NCM cells delivered around 30% higher specific capacities. With increasing rates, less capacity can be discharged from the cells, especially for the high C-rates of 2C and 3C. At a 2C discharge, only 88% can be discharged from the LMR-NCM cells and 77% from the NCA cells, when referenced to their capacity at C/10. At a 3C discharge, the LMR-NCM cells delivered 77%, while the NCA cells dropped to 59%. Previous studies with NCA^{38,39} and LMR-NCM^{10,40,41} showed that the capacity loss at high C-rates is largely due to the poor charge transfer kinetics and/or the slow solid-state diffusion at low SOC. However, it is noteworthy that the capacity loss with increasing C-rate was much more pronounced for LMR-NCM/lithium coin cells that were investigated in Part I of this study³⁵: at the same loading ($\approx 12 \text{ mg cm}^{-2}$) and cathode porosity ($\approx 42\%$), the capacity at 3C was only $\approx 120 \text{ mAh g}_{\text{CAM}}^{-1}$ (see Fig. 2 in Ref. 35), compared to the $\approx 180 \text{ mAh g}_{\text{CAM}}^{-1}$ obtained here for the LMR-NCM/graphite pouch cells (red symbols in Fig. 2a). As will be shown later, this was most likely linked to the strong cell temperature rise of the LMR-NCM pouch cells at high C-rates.

The mean discharge voltage at C/10 shown in Fig. 2b of the LMR-NCM cells was at 3.5 V, while it was at 3.7 V for the NCA cells. At a 3C rate, the mean discharge voltage of the LMR-NCM cells decreased by $\approx 660 \text{ mV}$, which was more than double compared to the $\approx 310 \text{ mV}$ drop of the NCA cells, revealing the strong rate dependency of the LMR-NCM CAM.

The gravimetric energy density of the pouch cells, displayed in Fig. 2c, is a product of the discharge capacity and the mean discharge voltage, referenced to the total mass of the pouch cells.

Table II. Sequence of the measurement procedures applied to the LMR-NCM/graphite and NCA/graphite pouch and coin cells.

Cycling procedure	Cycles	Charge	Stop condition	Discharge	Stop condition	
C/10 cycle	1	CC @ C/10	$U \geq U_{\max}$	CC @ C/10	$U \leq U_{\min}$	
C/10 relax cycle (initial OCV curve)	1	CC @ C/10 Pause	$t \geq 1$ h or $U \geq U_{\max}$ $t \geq 1$ h	CC @ C/10 Pause	$t \geq 1$ h or $U \leq U_{\min}$ $t \geq 1$ h	
Rate capability test	3	CC @ C/10 CV @ U_{\max}	$U \geq U_{\max}$ $I \leq C/20$	CC @ C/10	$U \leq U_{\min}$	
	3	CC @ C/5 CV @ U_{\max}	$U \geq U_{\max}$ $I \leq C/20$	CC @ C/5	$U \leq U_{\min}$	
	5	CC @ C/2 CV @ U_{\max}	$U \geq U_{\max}$ $I \leq C/20$	CC @ C/2	$U \leq U_{\min}$	
	Extended rate capability test ^{a)}	5	CC @ C/2 CV @ U_{\max}	$U \geq U_{\max}$ $I \leq C/20$	CC @ 1C	$U \leq U_{\min}$
		5	CC @ C/2 CV @ U_{\max}	$U \geq U_{\max}$ $I \leq C/20$	CC @ 2C	$U \leq U_{\min}$
		5	CC @ C/2 CV @ U_{\max}	$U \geq U_{\max}$ $I \leq C/20$	CC @ 3C	$U \leq U_{\min}$
Ageing cycles	25	CC @ C/2 CV @ U_{\max}	$U \geq U_{\max}$ $I \leq C/20$	CC @ C/2	$U \leq U_{\min}$	
Checkup procedure	Cycles	Procedure		Stop condition		
Initialization	1	CC charge @ C/10 Pause		$U \geq U_{\text{pulse}}$ $t \geq 1$ h		
Pulse Test	1	CC discharge @ C/2		$t \geq 10$ s		
C/10 cycle	1	CC discharge @ C/10 CC charge @ C/10 CC discharge @ C/10		$U \leq U_{\min}$ $U \geq U_{\max}$ $U \leq U_{\min}$		
1C cycle ^{a)}	3	CC charge @ C/2 CV charge @ U_{\max} CC discharge @ 1C		$U \geq U_{\max}$ $I \leq C/20$ $U \leq U_{\min}$		

Before the first stated C/10 cycle, the cells underwent a formation procedure consisting of one C/15 and two C/10 cycles. The C-rates refer to the nominal cell capacities listed in Table I. All measurements were performed at an ambient temperature of 25 °C. CC—constant current, CV—constant voltage. LMR-NCM: $U_{\max} = 4.6$ V, $U_{\min} = 2.0$ V, $U_{\text{pulse}} = 3.7$ V. NCA: $U_{\max} = 4.3$ V, $U_{\min} = 3.0$ V, $U_{\text{pulse}} = 3.7$ V. a) Two cells each were discharged with the extended rate capability test and the 1C checkup cycles.

At low discharge rates the energy density was around 200 Wh kg⁻¹ (≈ 433 Wh l⁻¹) for the LMR-NCM and 180 Wh kg⁻¹ (≈ 419 Wh l⁻¹) for the NCA pouch cells. In contrast to the 30% increase in specific capacity, the benefit in gravimetric energy density was only 11%. An adjusted N/P ratio of 1.17 for the NCA pouch cells (rather than the here used N/P ratio of 1.38) would result in 4% higher energy densities, reducing the energy density advantage of the LMR-NCM cells to 7%. One reason for the lower gain in energy density compared to the gain in capacity of the LMR-NCM cells was their lower mean discharge voltage. Nevertheless, in this study, the LMR-NCM pouch cells maintained a higher energy density of $\approx 11\%$ compared to the NCA pouch cells for C-rates up to 1C; this advantage became even more pronounced at higher rates of 2C (+16%) and 3C (+29%), which, as described later, is related to the substantial LMR-NCM cell temperature rise.

Both pouch cell types described in this work were not designed for a specific application or optimized with regards to their energy density. High energy cells use thinner current collectors and separators as well as lower electrode porosities, which requires less electrolyte.^{29,33} All these measures save weight and volume and thereby increase the gravimetric and volumetric energy density on the cell level. Based on the cylindrical cells for EVs reported by Ding et al.³⁰ with 236 Wh kg⁻¹ (NCA/graphite) and 260 Wh kg⁻¹ (NCA/silicon-graphite), by switching the CAM from NCA to LMR-NCM and assuming a gravimetric energy density increase of 7% compared

to the properly balanced NCA/graphite or NCA/silicon-graphite cells, 253 Wh kg⁻¹ (LMR-NCM/graphite) and 278 Wh kg⁻¹ (LMR-NCM/silicon-graphite) could be reached.

The performance of the laboratory coin cells served as a comparison for the large-format multilayer pouch cells. As already mentioned above with regards to the discharge rate capability test, the LMR-NCM/graphite coin cells (as well as the LMR-NCM/lithium coin cells measured in Part I³⁵) showed a specific capacity that was $\approx 34\%$ lower than that of the corresponding pouch cells for a 3C discharge (see Fig. 3a). In contrast, the specific capacity of the NCA laboratory coin cells was in good agreement for all C-rates with the NCA pouch cells (see solid gray squares and open gray triangles in Fig. 3a). Just for clarification, for the 2C and 3C discharge in Fig. 3a, the open gray triangles indicating the specific capacity of the NCA coin cells are superposed by the open red triangles for the LMR-NCA coin cells.

While the coin cells can be considered isothermal at an ambient temperature of 25 °C during operation due to their low energy content and high thermal mass, this is not the case for large-format pouch cells. The maximum temperature of the pouch cells was reached at the end of each discharge and is depicted in Fig. 3b. As described in the experimental section, the temperature was measured on the surface of the pouch cells within the cell holder (see Fig. 1). The cell holder, consisting partly of aluminum and the thermoplastic POM, influenced the heat dissipation of the cells. As there were no

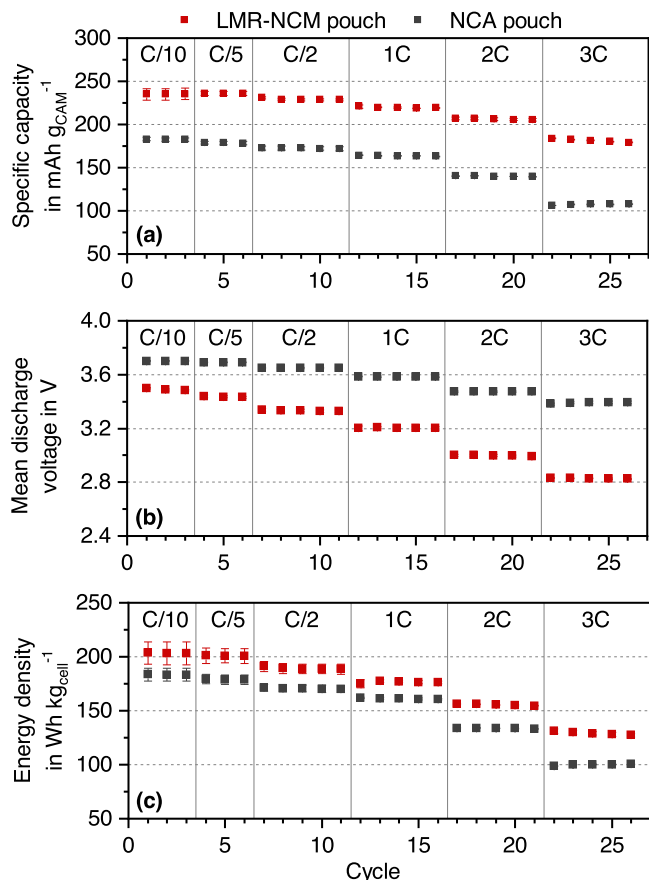


Figure 2. Discharge rate capability of the LMR-NCM and NCA pouch cells (as specified in Table I), depicting the C-rate dependence of (a) the specific capacity related to the CAM mass, (b) the mean cell discharge voltage, and (c) the energy density with respect to the total mass of the cell. The cells were discharged with a CC procedure at an ambient temperature of 25 °C in the voltage windows 4.6–2.0 V for LMR-NCM and 4.3–3.0 V for NCA, respectively (see Table II). The error bars for the rates of C/10, C/5, and C/2 represent the standard deviation between 5 LMR-NCM and 6 NCA cells; for the rates of 1C, 2C, and 3C, the error bars mark the minimum/maximum values of 2 cells of each type.

rest periods at the end of discharge during the rate capability test, the cells could not cool down to the 25 °C ambient temperature of the climate chamber and had an initial temperature of around 27.5 °C at the beginning of the rate capability test (see Fig. 3b). The temperature of the LMR-NCM cells strongly increased with increasing C-rates, reaching a temperature of 53 °C for the 3C discharge, while the NCA cells only reached 33 °C.

Figure 3c displays the round-trip energy efficiencies of both the LMR-NCM and NCA pouch and coin cells. The generated heat in a cell can be correlated to the energy that is irreversibly lost between

charge and discharge. After formation, this energy inefficiency is mainly caused by a voltage hysteresis between charge and discharge and therefore pronounced in LMR-NCM cells.⁴² During the 3C discharge (following a C/2 CCCV charge, see Table II), the energy loss of the LMR-NCM pouch cells was above 6 Wh (corresponding to an energy efficiency of ≈70%), while the NCA pouch cells only lost around 2 Wh (corresponding to an energy efficiency of ≈85%). Table IV lists the mean charge (E_{CH}) and discharge (E_{DCH}) energies of the LMR-NCM and NCA pouch cells vs discharge rate (DCH C-rate) as well as the resulting round-trip energy efficiencies (η), defined as

$$\eta = \frac{E_{DCH}}{E_{CH}} \cdot 100\% \quad [1]$$

It also lists the overall dissipated energy per cycle (ΔE_{tot})

$$\Delta E_{tot} = E_{CH} - E_{DCH} \quad [2]$$

Meister et al.⁴² classified different anode and cathode materials according to their round-trip energy efficiency for a 1C charge/discharge cycle at an ambient temperature of 20 °C. In their study, graphite had a round-trip energy efficiency of ≈94%, their LMR-NCM (0.5 Li₂MnO₃ · 0.5 LiNi_{0.4}Mn_{0.4}Co_{0.2}O₂) had a round-trip energy efficiency of ≈85%, while NCA was not investigated. Their LMR-NCM/graphite combination would result in a round-trip energy efficiency of ≈80%. This round-trip energy efficiency at a 1C rate reflects the results for the LMR-NCM/graphite pouch cells obtained in our study (≈81% at 1C). Note that these values were measured at an ambient temperature of 20 °C, while our measurements were performed at an ambient temperature of 25 °C.

To further evaluate the difference in round-trip energy efficiency of both cell types, the charge and discharge voltage profiles of each cell type have to be closer examined. The total energy loss related to voltage hysteresis can be split into a resistive part ΔE_R , due to cell polarization during operation, and into a current-independent part ΔE_{OCV} , originating from the intrinsic active material voltage hysteresis that is particularly pronounced for LMR-NCMs.^{26,42}

$$\Delta E_{tot} = \Delta E_R + \Delta E_{OCV} \quad [3]$$

The additional energy that is lost due to parasitic side reactions was neglected in our estimation of the energy losses, as they are minor for the high coulombic efficiencies >99.9% for both cell types in our study. The reversible heat (entropy) during a full charge/discharge cycle is considered close to zero (under the assumption that no net entropy can be generated in a reversibly cyclable cell) and therefore insignificant for the total energy loss.

For the evaluation of the energy losses, a C/10 charge/discharge cycle with and without intermittent 1 h OCV rest periods was carried out. The LMR-NCM pouch cells were cycled in a voltage range of 2.0–4.6 V and the NCA pouch cells in a voltage range of 3.0–4.3 V, the results are displayed in Fig. 4. Clearly visible is the pronounced hysteresis of the voltage profile of the LMR-NCM cells. When OCV rest periods are added to the C/10 cycling, represented by the red lines, the purely resistive part is omitted. The cell voltage is allowed

Table III. Specific CAM capacity, mean cell discharge voltage, and gravimetric cell-level energy density of the LMR-NCM and NCA pouch cells. The values for the C-rates were referenced to their mean C/10 value and the corresponding standard deviation, based on the data shown in Fig. 2.

	Cell type	C/5	C/2	1C	2C	3C
Specific capacity	LMR-NCM	100.4 ± 2.9 %	97.6 ± 2.8 %	93.5 ± 2.7 %	87.8 ± 2.5 %	77.3 ± 2.2 %
	NCA	97.9 ± 1.1 %	94.4 ± 1.1 %	89.6 ± 1.0 %	76.7 ± 0.9 %	58.8 ± 0.7 %
Mean dis. voltage	LMR-NCM	98.5 ± 0.2 %	95.5 ± 0.2 %	91.8 ± 0.2 %	85.9 ± 0.2 %	81.1 ± 0.2 %
	NCA	99.7 ± 0.1 %	98.6 ± 0.1 %	96.8 ± 0.1 %	93.9 ± 0.1 %	91.6 ± 0.1 %
Energy density	LMR-NCM	99.1 ± 5.1 %	93.3 ± 4.8 %	87.0 ± 4.5 %	76.7 ± 4.0 %	63.7 ± 3.3 %
	NCA	97.7 ± 3.2 %	93.1 ± 3.0 %	88.0 ± 2.8 %	73.0 ± 2.4 %	54.6 ± 1.8 %

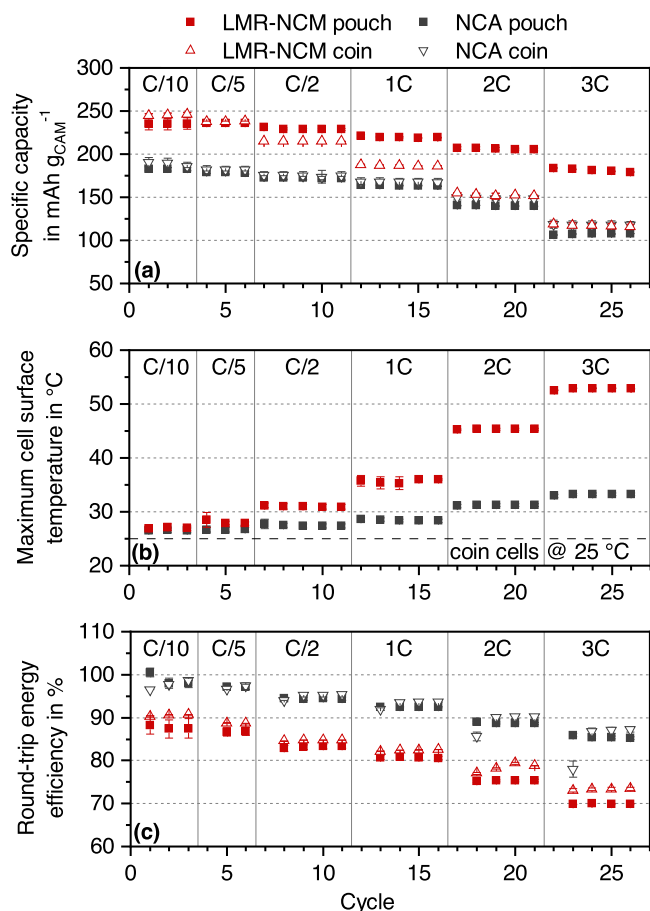


Figure 3. (a) Specific capacity related to the CAM mass of the LMR-NCM and NCA pouch cells in comparison to the laboratory coin cell measurements (all with graphite anodes), (b) maximum temperature measured on the surface of the pouch cells within the cell holder, and (c) round-trip energy efficiency calculated from the ratio of charge and discharge energy in a given cycle (note that the first cycle for each new C-rate setting is omitted). The pouch cell data correspond to those depicted in Fig. 2. The error bars for the coin cell measurements (barely visible) represent the standard deviation between 3 individual coin cells of each type.

to relax and the tips of the red curve mark the OCV profile after 1 h rest periods. A connection of these tips leave the gray shaded area that indicates the energy lost due to the LMR-NCM material hysteresis. The voltage profile of the NCA cells showed a minor

hysteresis, which almost vanished completely when OCV rest periods were added to the cycling procedure. For this reason, the gray area in Fig. 4b is quasi not visible and appears as the dotted gray line. Via integration of the C/10 charge/discharge cycle, the energy loss ΔE_{tot} can be derived.²⁶

$$\Delta E_{\text{tot}} = \oint I V dt \quad [4]$$

Here, I and V refer to the cell current and voltage, respectively. An integration of the gray shaded areas in Fig. 4 yields ΔE_{OCV} . ΔE_{R} is then calculated using Eq. 3 and ΔE_{tot} determined from the black dashed lines in Fig. 4, using Eq. 4. The results are listed in Table V. These energy values, obtained by integration of the voltage curve of a single pouch cell of each type, are in good agreement with the measured C/10 round-trip efficiencies during the rate capability test, as stated in Table IV ($87.5\% \pm 2.2\%$ for the LMR-NCM and $98.1\% \pm 1.1\%$ for the NCA pouch cells).

The total energy ΔE_{tot} that was lost over one C/10 charge/discharge cycle was substantially less for the NCA pouch cell, accounting for 2.3% of the charge energy E_{CH} . In contrast, the LMR-NCM cell lost 13.5% of the charge energy. More than a third of the total losses in the LMR-NCM cells at C/10 could be attributed to the intrinsic LMR-NCM material OCV hysteresis, whereas the ratio $\Delta E_{\text{OCV}}/\Delta E_{\text{tot}}$ was only 7% for the NCA cells. The NCA voltage hysteresis was almost only generated by overpotential contributions (ΔE_{R}).

The energy lost due to the OCV hysteresis of the LMR-NCM pouch cells caused the pronounced temperature rise visible in Fig. 3b. For lower discharge currents, there was enough time to dissipate the excess heat to the cell holders and the ambient air. If the same energy is released in a short time period, it cannot dissipate fast enough, resulting in an increasing cell temperature. The OCV voltage hysteresis of LMR-NCM and the resulting energy inefficiency are major drawbacks for commercialization and are thus in the focus of current research.²⁶ Regarding the discharge capacities and the round-trip energy efficiencies in the rate capability test, LMR-NCM is rather suited for high energy than high power applications.

Cycling behavior.—In the aging study (see Figs. 5 and 6), the large-format LMR-NCM and NCA pouch cells were evaluated with regards to their cycling behavior, using diagnostic checkups every 25 cycles. The dashed lines in Figs. 5a and 5c mark the 80% state-of-health (SOH) thresholds for the specific capacity and energy density, referenced to 80% of the initial capacity and cell energy density during the C/2 discharge in the rate capability test (i.e., 80% of the values in cycle 7 shown in Figs. 2a and 2c). With ongoing cycling, both the LMR-NCM and the NCA cells showed a gradual decline in their specific capacity.

Table IV. Mean round-trip energy efficiencies η of the LMR-NCM and NCA pouch cells (data shown in Figs. 2 and 3), listed here for the third cycle of each discharge C-rate. The details of the discharge rate capability test are given in Table II.

Type	DCH C-rate	E_{CH}	E_{DCH}	ΔE_{tot}	η
LMR-NCM	C/10	26.6 Wh	23.3 Wh	3.33 Wh	$87.5\% \pm 2.2\%$
	C/5	26.2 Wh	22.7 Wh	3.46 Wh	$86.8\% \pm 1.0\%$
	C/2	25.5 Wh	21.2 Wh	4.31 Wh	$83.1\% \pm 0.6\%$
	1C	24.2 Wh	19.5 Wh	4.64 Wh	$80.8\% \pm 0.5\%$
	2C	22.7 Wh	17.1 Wh	5.62 Wh	$75.3\% \pm 0.3\%$
	3C	20.3 Wh	14.2 Wh	6.10 Wh	$70.0\% \pm 0.1\%$
NCA	C/10	21.9 Wh	21.5 Wh	0.42 Wh	$98.1\% \pm 1.1\%$
	C/5	21.4 Wh	20.8 Wh	0.62 Wh	$97.1\% \pm 0.7\%$
	C/2	20.9 Wh	19.8 Wh	1.17 Wh	$94.4\% \pm 0.4\%$
	1C	20.0 Wh	18.5 Wh	1.51 Wh	$92.4\% \pm 0.2\%$
	2C	17.3 Wh	15.3 Wh	1.94 Wh	$88.7\% \pm 0.3\%$
	3C	13.5 Wh	11.5 Wh	1.96 Wh	$85.4\% \pm 0.3\%$

CH—charge, DCH—discharge, tot—total.

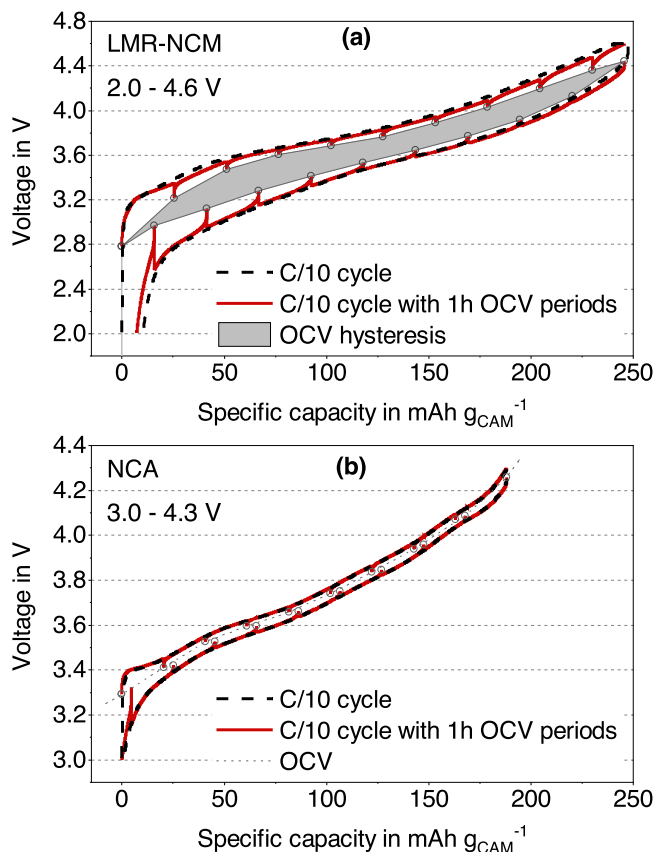


Figure 4. C/10 cycle procedures with and without 1 h OCV rest periods (see Table II) of an (a) LMR-NCM (2.0–4.6 V) and a (b) NCA (3.0–4.3 V) pouch cell at an ambient temperature of 25 °C.

After approximately 250 cycles, too much gas was generated in the LMR-NCM pouch cells, which caused a rupture of the pouch foil. The strong gassing of the LMR-NCM cells likely derives from two effects: i) the oxidative decomposition of the electrolyte due to its reaction with released lattice oxygen at the very high degrees of delithiation of the LMR-NCM at 100% SOC⁴³; ii) the gradual thermal decomposition of FEC,⁴⁴ which is particularly problematic for electrolytes with high FEC content. While we did not determine the gas composition, the literature suggests the evolution of mostly CO₂ at room temperature and over a few cycles with FEC based electrolytes,^{36,45} whereas at elevated temperatures and over extended cycling in FEC/DEC (2:8 by volume) electrolyte also substantial amounts of H₂ were observed.⁴⁶ Even though the electrochemical behavior of the cells was still stable, the tests were stopped for safety reasons.

The NCA cells showed a more stable cycling behavior. For a better comparison of the two active materials, the NCA cell data are only plotted up to 300 cycles in Fig. 5; an overview of all the data up to 1600 cycles for the NCA pouch cells and up to 1000 cycles for the NCA coin cells is given in the Appendix in Fig. A-2, indicating the state-of-the-art performance of the large-format multilayer pouch cells. While the upscaling from coin to pouch cells for a state-of-the-art reference material is adequate, effects related to temperature and

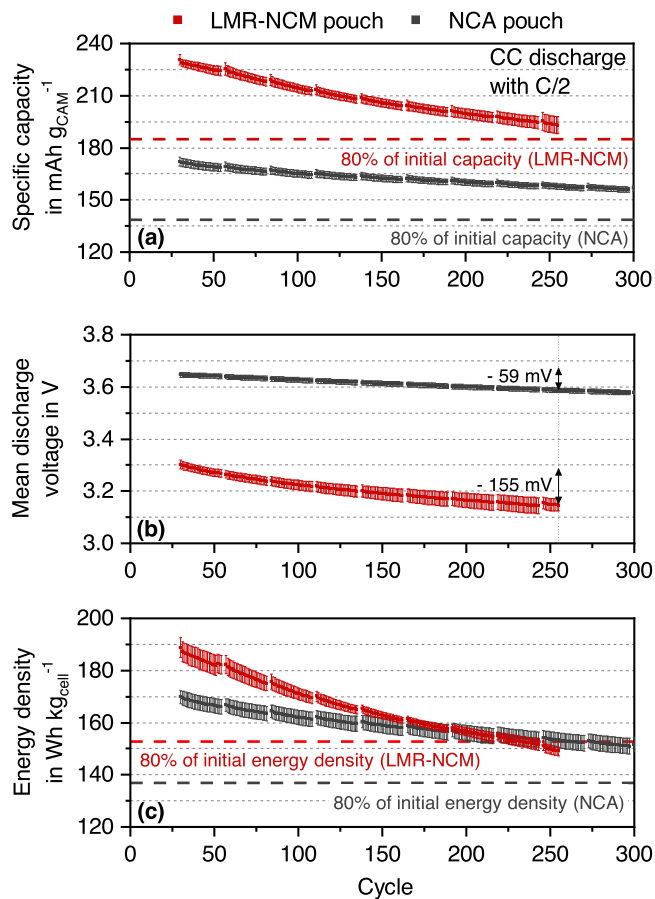


Figure 5. Cycle stability of the LMR-NCM and NCA pouch cells with regards to their (a) specific capacity related to the CAM mass, (b) mean cell discharge voltage, and (c) energy density related to the total mass of the cell. The cells were charged and discharged with a C/2 CC procedure including a CV phase at the end of charge at an ambient temperature of 25 °C in the voltage windows 2.0–4.6 V for LMR-NCM and 3.0–4.3 V for NCA, respectively (see Table II). Shown are the average values from 6 LMR-NCM and 5 NCA pouch cells, with error bars representing the standard deviation. The 80% initial capacity and energy density values marked by the dashed horizontal lines are referenced to the respective values in cycle 7 shown in Figs. 2a and 2c.

gas evolution that occur in LMR-NCM cells can clearly not be appropriately predicted from coin cell data, as they are operated isothermally and do not capture cell rupture effects from extensive gassing. Furthermore, small-scale laboratory cells generally have a higher electrolyte to active material ratio³⁵ that affects the aging behavior, which likely explains the slightly better capacity retention of the NCA coin vs NCA pouch cells (see Fig. A-2).

The specific capacity of the LMR-NCM pouch cells decreased faster, but remained higher than for the NCA pouch cells as shown in Fig. 5a. An extrapolation of the specific capacity of the LMR-NCM cells projects a crossover with the 80% threshold at approximately 350 cycles, as seen in Fig. A-1 in the Appendix. The NCA cells reached this point after 980 cycles (see Fig. A-2), as is also listed in Table VI. The aging behavior of both cell types is in good agreement

Table V. Energy losses derived from integrating the C/10 cycling curves. The total energy loss is divided into the hysteresis (ΔE_{OCV}) and the overpotential (ΔE_R) driven part.

Cell type	ΔE_{tot}	ΔE_{OCV}	ΔE_R	$\Delta E_{OCV} : \Delta E_R$	η	$\Delta E_{tot}/E_{CH}$
LMR-NCM	3.54 Wh	1.31 Wh	2.23 Wh	37 : 63	86.5%	13.5%
NCA	0.50 Wh	0.04 Wh	0.46 Wh	7 : 93	97.7%	2.3%

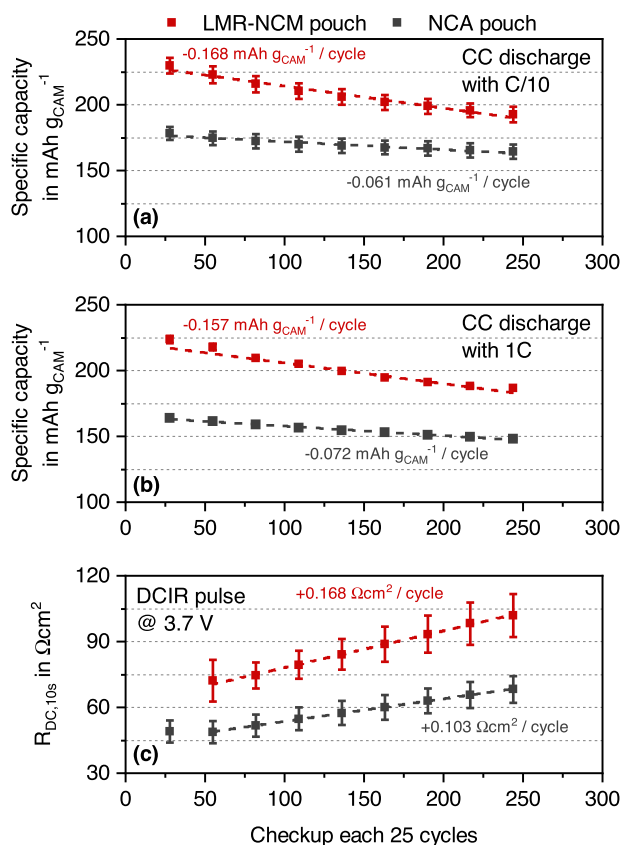


Figure 6. Checkup cycles (see Table II) of the LMR-NCM and NCA pouch cell tests shown in Fig. 5 with regards to their (a) specific C/10 discharge capacity related to the CAM mass, (b) specific 1C discharge capacity related to the CAM mass, and (c) DCIR for a 10 s C/2 discharge after charging the cells to a voltage of 3.7 V. The dashed lines indicate a linear regression of the mean values of the data points. In (a) and (c), average values from 6 LMR-NCM and 5 NCA pouch cells are shown, and the error bars represent the standard deviation. In (b), only average values of 2 cells of each type are shown, with the error bars representing their minimum/maximum values.

with published data on core-shell or surface-coated LMR-NCM in LMR-NCM/graphite cells^{11,12} and of NCA in NCA/graphite cells.^{6,47–49}

In Fig. 5b, the mean discharge voltage of the NCA cells showed a decrease of 59 mV after 255 cycles, which was less pronounced than the loss of 155 mV of the LMR-NCM cells. Voltage fading during prolonged cycling is a known issue of LMR-NCM and is caused by structural reordering from a layered to a spinel-like structure.^{11,12,27,50–53} This has an additional, negative impact on the energy density decay displayed in Fig. 5c. In the beginning of the cycle-life test, the LMR-NCM cells offered a 11% higher cell energy density, but due to their faster degradation, their cell energy density became the same as that of the NCA cells at cycle 210. After 230 cycles, the LMR-NCM cells reached their 80% SOH criterion (red dashed line in Fig. 5c), whereas the NCA cells could be cycled 710 times until they reached 80% SOH (gray dashed line in Fig. 5c). The number of cycles up to 80% SOH with regards to their specific capacity and energy density for the two cell types are summarized in Table VI. Note that the LMR-NCM cells were charged to 4.6 V while the NCA cells were only charged to 4.3 V. At such high voltages, the electrolyte stability plays an important role and determines the aging behavior of these cells. Electrolyte oxidation at the cathode was probably one cause for an accelerated aging.^{36,43,45} While higher temperatures also lead to an accelerated aging of lithium-ion cells,^{47,54–57} this would not explain the comparatively faster degradation of the LMR-NCM cells since their average surface temperature during this aging test at C/2 of 29 °C (max. 31 °C) was similar to the 27 °C of that of the NCA cells (max. 28 °C).

Table VI. C/2 cycling stability defined by the 80% SOH criterion of the LMR-NCM and NCA pouch cells based on the data shown in Fig. 5.

80% SOH	LMR-NCM	NCA
Specific capacity	350 cycles ^{a)}	980 cycles
Energy density	230 cycles	710 cycles

a) extrapolation, see Fig. A-1 in the Appendix.

During the checkup cycles, the remaining capacity was assessed by a C/10 cycle, displayed in Fig. 6a. By applying a lower current, the cell polarization due to internal resistances, e.g., caused by growing passive layers or contact losses, is less. The influence of the internal resistance buildup on the capacity was evaluated with an additional 1C discharge, as seen in Fig. 6b. As described in the experimental section, only two pouch cells of each type were stressed with the 1C cycling procedure and therefore smaller error bars appear in Fig. 6b. By comparing the capacity of the C/10 with the 1C discharge, the capacity fading of the LMR-NCM cells is essentially independent of the C-rate, which suggests that the main degradation mechanism is the loss of cyclable lithium (e.g., via electrolyte oxidation) rather than an impedance buildup, at least for discharge C-rates up to 1C. For the NCA cells, the capacity fading at 1C is only ≈20% faster than at C/10, again suggesting that this decrease is not dominated by an impedance buildup.

The DCIR method was used to determine the internal cell resistance, employing a discharge pulse after a relaxation time of 1 h at 3.7 V (see Table II), which corresponded to a SOC of about 40% for both cell types. The first checkup of the LMR-NCM cells before the aging study was measured at a different voltage and was therefore left out. Here it should be noted, however, that the cell resistance is a strong function of SOC and thus cell voltage for both LMR-NCM¹⁰ and for NCA⁶ with a minimum resistance at mid-range SOCs. Based on the cathode-resolved impedance of NCM-811,⁵⁸ this resistance versus SOC behavior reflects that of the CAM. Moreover, because of the strong voltage hysteresis for LMR-NCM, the resistance also depends on whether the cell was charged or discharged before applying a DCIR pulse.¹⁰ While the LMR-NCM cells exhibited ≈2-fold higher resistances, the resistances of both cell types rose equally by ≈40% between the 50th and the 250th cycle.

Therefore, the faster capacity and cell energy density degradation of the LMR-NCM cells compared to the NCA cells is unlikely due to polarization effects. Instead, based on the similar capacity fading rates of C/10 and 1C for both cell types (Figs. 6a and 6b), the performance degradation seems to be due to a loss of cyclable lithium. That the latter would be more pronounced at the higher cathode potentials of the LMR-NCM cells is not surprising, enhanced by the reaction of the electrolyte with lattice oxygen at the high degrees of delithiation at 100% SOC for this material.⁴³ Therefore, a more stable electrolyte system is still required for LMR-NCM CAMs, particularly for elevated temperatures due to the thermal instabilities of FEC in combination with LiPF₆.^{44,46} Moreover, surface modifications of LMR-NCM materials could also reduce detrimental side reactions and improve the overall cycling stability.^{11,12}

Conclusions

In this study, the LMR-NCM cathode active material, offering a high reversible capacity of 250 mAh g⁻¹, was employed with graphite anodes in large-format multilayer pouch cells, which were produced on a pilot scale production line. Comparable NCA/graphite pouch cells were produced and served as a reference for an evaluation of the performance of the LMR-NCM cells. The two pouch cell types were standardized to deliver an areal capacity of 2.3 mAh cm⁻² or a total capacity of 5.5 Ah at a 1C discharge rate.

The characteristics of both cell types were compared against each other in a discharge rate capability test and an aging test.

Distinct differences between the two cell types were the wider voltage window of the LMR-NCM cells with a lower cutoff voltage of 2.0 V and an upper cutoff voltage of 4.6 V as well as the hysteresis of the voltage profile between charge and discharge even at C/10, while the NCA cells were cycled between 3.0–4.3 V and showed almost no voltage hysteresis. The LMR-NCM cells exhibited a specific capacity of 235 mAh g^{-1} for low discharge currents $\leq C/5$, which amounted to a 30% increase compared to the 180 mAh g^{-1} of the NCA cells. However, because of the voltage hysteresis and the lower mean discharge voltage, the energy density of the LMR-NCM pouch cells was only $\approx 11\%$ higher in comparison to the NCA cells.

The aging behavior was evaluated with a C/2 cycling test and initially showed a better performance of the LMR-NCM cells. However, both the specific capacity and the energy density showed a faster degradation, so that the LMR-NCM pouch cells were projected to reach their 80% SOH criterion with respect to the specific capacity after approximately 350 cycles, whereas the 80% of the initial energy density was reached after already 230 cycles, due to a faster voltage fading. On the other hand, these 80% SOH criteria were reached after 980 cycles and 710 cycles, respectively for the NCA cells. Checkup cycles including the measured cell resistances showed that the increasing cell resistance was not dominating the overall capacity decay, and that instead the performance degradation of both the LMR-NCM and the NCA cells is rather due to a loss of cyclable lithium. The overall cycle life of the LMR-NCM pouch cells was limited to ≈ 250 cycles due to cell rupture caused by the strong gassing of the LMR-NCM cells.

In conclusion, LMR-NCM proved to be a high capacitive CAM, which is comparatively cheap because of its high manganese share compared to cobalt and nickel. Long-term stability issues still have to be addressed, e.g., a surface treatment of LMR-NCM could bring improvements on the material level, and should be examined in combination with an adequate electrolyte system. Because of the heat accumulation for discharge rates above C/2, an application of LMR-NCM in large-format cells should be critically assessed together with the accompanying cooling system. This issue will be addressed in our future research. Generally, the material is more suited for high energy than high power applications.

Acknowledgments

This work was financially supported by the German Federal Ministry of Education and Research (BMBF) under grant number 03XP0081 (ExZellTUM II) and 03XP0255 (ExZellTUM III). For the production of the large-format pouch cells, special thanks go to the battery production research team of iwB, in particular to Benedikt Stumper, Ajinkya Metkar, Nicolas Billot, Till Günther, Johannes Kriegler, Fabian Konwitschny, Celestine Singer, Hoda Mohseni, Sophie Grabmann, and Joscha Schnell. The authors gratefully acknowledge Tobias Teufl and Manuel Mendez from BASF SE for the helpful scientific discussions, Robin Schregle for his contribution to the CAD drawing of the cell holder, and Fabian Linsenmann for his critical feedback.

Appendix

The measured cycling data of the LMR-NCM pouch cells was limited to approximately 250 cycles due to gassing induced rupture of the cells. To have an assessment of the 80% SOH criterion regarding the specific capacity of the cells, an extrapolation was carried out, yielding a projected crossover after approximately 350 cycles (see Fig. A-1). The following fitting function ($R^2 = 0.9986$) was used for this extrapolation (see black line in Fig. A-1), with x representing the cycle number and y the specific capacity in $\text{mAh g}_{\text{CAM}}^{-1}$:

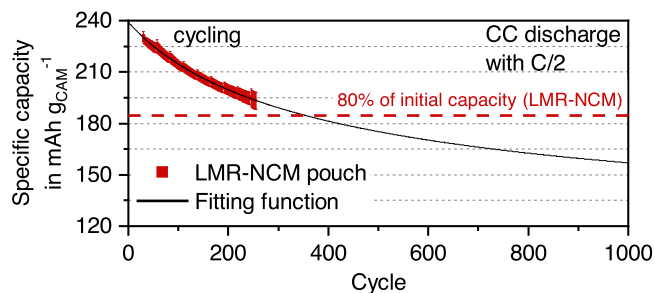


Figure A-1. Extrapolation of the specific capacity related to the mass of the active material during C/2 cycling of the LMR-NCM pouch cells.

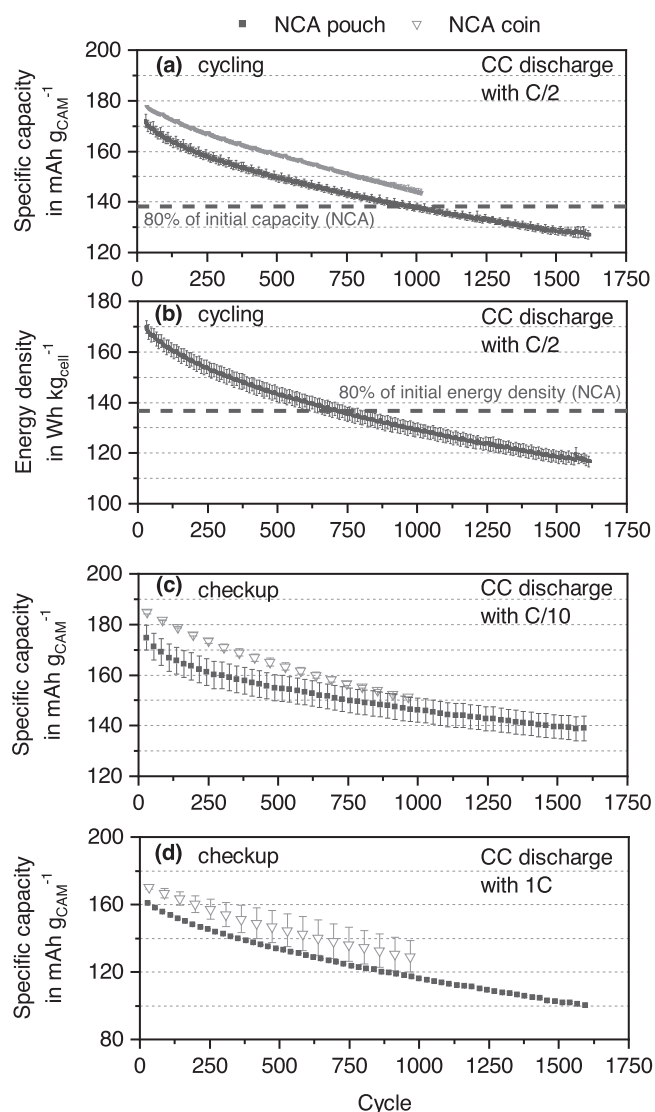


Figure A-2. Cycle stability including all cycles and checkups of the NCA pouch and coin cells. (a) Specific capacity related to the mass of the active material and (b) energy density related to the total mass of the cell during C/2 cycling (only displayed for the NCA pouch cells). (c) Specific C/10 discharge capacity and (d) specific 1C discharge capacity related to the mass of the active material during the checkups every 25 C/2 cycles. The cells were charged with a C/2 CC procedure including a CV phase at the end of charge at an ambient temperature of 25°C in the voltage window 3.0–4.3 V (see Table II).

$$y = \frac{2107}{\sqrt{218.8 + x}} + 96.61 \quad [\text{A-1}]$$

To allow for a more clear comparison between the LMR-NCM and the NCA cells, Fig. 5 only shows the initial 300 cycles for the NCA cells. The total cycling stability of the NCA pouch cells including the laboratory NCA coin cells is displayed in Fig. A-2. The coin cells were cycled up to 1000 cycles while the pouch cell aging test was carried out for over 1600 cycles. The energy density in Fig. A-2b is only displayed for the pouch cells, because this value is related to the total cell mass, which is not representative for coin cells.

ORCID

Ludwig Kraft  <https://orcid.org/0000-0003-4324-426X>
 Tanja Zünd  <https://orcid.org/0000-0002-1650-3636>
 David Schreiner  <https://orcid.org/0000-0001-8035-0438>
 Rebecca Wilhelm  <https://orcid.org/0000-0002-4161-5197>
 Florian J. Günter  <https://orcid.org/0000-0002-5967-6801>
 Hubert A. Gasteiger  <https://orcid.org/0000-0001-8199-8703>
 Andreas Jossen  <https://orcid.org/0000-0003-0964-1405>

References

- D. Andre, S.-J. Kim, P. Lamp, S. F. Lux, F. Maglia, O. Paschos, and B. Staszny, "Future generations of cathode materials: an automotive industry perspective." *Journal of Materials Chemistry A*, **3**, 6709 (2015).
- S.-T. Myung, F. Maglia, K.-J. Park, C. S. Yoon, P. Lamp, S.-J. Kim, and Y.-K. Sun, "Nickel-rich layered cathode materials for automotive lithium-ion batteries: achievements and perspectives." *ACS Energy Lett.*, **2**, 196 (2017).
- M. A. Hannan, M. M. Hoque, A. Mohamed, and A. Ayob, "Review of energy storage systems for electric vehicle applications: issues and challenges." *Renew. Sustain. Energy Rev.*, **69**, 771 (2017).
- R. Schmich, R. Wagner, G. Höppl, T. Placke, and M. Winter, "Performance and cost of materials for lithium-based rechargeable automotive batteries." *Nat. Energy*, **3**, 267 (2018).
- C. S. Yoon, K.-J. Park, U.-H. Kim, K. H. Kang, H.-H. Ryu, and Y.-K. Sun, "High-energy Ni-rich Li[Ni_xCo_{1-x-y}Mn_{1-x-y}]O₂ cathodes via compositional partitioning for next-generation electric vehicles." *Chemistry of Materials*, **29**, 10436 (2017).
- R. Weber, A. J. Louli, K. P. Plucknett, and J. R. Dahn, "Resistance growth in lithium-ion pouch cells with LiNi_{0.80}Co_{0.15}Al_{0.05}O₂ positive electrodes and proposed mechanism for voltage dependent charge-transfer resistance." *J. Electrochem. Soc.*, **166**, A1779 (2019).
- S. Hwang and E. A. Stach, "Using in situ and operando methods to characterize phase changes in charged lithium nickel cobalt aluminum oxide cathode materials." *J. Phys. D*, **53**, 113002 (2020).
- J. R. Croy, M. Balasubramanian, K. G. Gallagher, and A. K. Burrell, "Review of the U.S. department of energy's deep effort to understand voltage fade in Li- and Mn-rich cathodes." *Acc. Chem. Res.*, **48**, 2813 (2015).
- G. E. Blomgren, "The development and future of lithium ion batteries." *J. Electrochem. Soc.*, **164**, A5019 (2016).
- T. Teuffl, D. Pritzl, S. Solchenbach, H. A. Gasteiger, and M. A. Mendez, "State of charge dependent resistance build-up in Li- and Mn-rich layered oxides during lithium extraction and insertion." *J. Electrochem. Soc.*, **166**, A1275 (2019).
- D. Becker, M. Börner, A. Friesen, S. Klein, U. Rodehorst, M. Diehl, M. Winter, T. Placke, and R. Schmich, "Towards high-performance Li-rich NCM—graphite cells by germanium-polymer coating of the positive electrode material." *J. Electrochem. Soc.*, **167**, 060524 (2020).
- J. Helbig, T. Beuse, V. Sizios, T. Placke, M. Winter, and R. Schmich, "Li—Mn-rich cathode materials with low-cobalt content and core-shell particle design for high-energy lithium ion batteries." *J. Electrochem. Soc.*, **167**, 060519 (2020).
- K. G. Gallagher and P. A. Nelson, "Manufacturing costs of batteries for electric vehicles." *Lithium-Ion Batteries: Advances and Applications*, ed. G. Pistoia (Elsevier, Amsterdam) p. 97 (2014).
- O. Gröger, H. A. Gasteiger, and J.-P. Suchsland, "Review—electromobility: batteries or fuel cells?" *J. Electrochem. Soc.*, **162**, A2605 (2015).
- A. Kwade, W. Haselrieder, R. Leithoff, A. Modlinger, F. Dietrich, and K. Droeder, "Current status and challenges for automotive battery production technologies." *Nat. Energy*, **3**, 290 (2018).
- UK Electric Vehicle and Battery Production Potential to 2040. March 2020. <https://faraday.ac.uk/publications/ev-economics-study/>.
- SMM Information & Technology Co, Ltd., Nickel price. Accessed 2/9/2021 <https://price.metal.com/Nickel>.
- SMM Information & Technology Co, Ltd., Manganese price. Accessed 2/9/2021 <https://price.metal.com/Manganese>.
- Y.-K. Sun, D.-J. Lee, Y. J. Lee, Z. Chen, and S.-T. Myung, "Cobalt-free nickel rich layered oxide cathodes for lithium-ion batteries." *ACS Applied Materials & Interfaces*, **5**, 11434 (2013).
- N. Zhang, N. Zaker, H. Li, A. Liu, J. Inglis, L. Jing, J. Li, Y. Li, G. A. Botton, and J. R. Dahn, "Cobalt-free nickel-rich positive electrode materials with a core-shell structure." *Chemistry of Materials*, **31**, 10150 (2019).
- H. Li, M. Cormier, N. Zhang, J. Inglis, J. Li, and J. R. Dahn, "Is cobalt needed in ni-rich positive electrode materials for lithium ion batteries?" *J. Electrochem. Soc.*, **166**, A429 (2019).
- W.-C. Chen, Y.-F. Song, C.-C. Wang, Y. Liu, D. T. Morris, P. A. Pianetta, J. C. Andrews, H.-C. Wu, and N.-L. Wu, "Study on the synthesis-microstructure-performance relationship of layered Li-excess nickel-manganese oxide as a Li-ion battery cathode prepared by high-temperature calcination." *Journal of Materials Chemistry A*, **1**, 10847 (2013).
- Trading Economics, Cobalt price. Accessed 2/9/2021 <https://tradingeconomics.com/commodity/cobalt>.
- Trading Economics, Lithium price. Accessed 2/9/2021 <https://tradingeconomics.com/commodity/lithium>.
- Trading Economics, Aluminum price. Accessed 2/9/2021 <https://tradingeconomics.com/commodity/aluminum>.
- G. Assat, S. L. Glazier, C. Delacourt, and J.-M. Tarascon, "Probing the thermal effects of voltage hysteresis in anionic redox-based lithium-rich cathodes using isothermal calorimetry." *Nat. Energy*, **4**, 647 (2019).
- N. Leifer, T. Penki, R. Nanda, J. Grinblat, S. Luski, D. Aurbach, and G. Goobes, "Linking structure to performance of Li_{1.2}Mn_{0.54}Ni_{0.13}Co_{0.13}O₂ (Li and Mn rich NMC) cathode materials synthesized by different methods." *Physical Chemistry Chemical Physics: PCCP*, **22**, 9098 (2020).
- J. B. Quinn, T. Waldmann, K. Richter, M. Kasper, and M. Wohlfahrt-Mehrens, "Energy density of cylindrical li-ion cells: a comparison of commercial 18650 to the 21700 cells." *J. Electrochem. Soc.*, **165**, A3284 (2018).
- M. J. Lain, J. Brandon, and E. Kendrick, "Design strategies for high power vs high energy lithium ion cells." *Batteries*, **5**, 64 (2019).
- Y. Ding, Z. P. Cano, A. Yu, J. Lu, and Z. Chen, "Automotive li-ion batteries: current status and future perspectives." *Electrochemical Energy Reviews*, **2**, 1 (2019).
- H. Popp, N. Zhang, M. Jahn, M. Arrinda, S. Ritz, M. Faber, D. U. Sauer, P. Azais, and I. Cendoya, "Ante-mortem analysis, electrical, thermal, and ageing testing of state-of-the-art cylindrical lithium-ion cells." *E & I Elektrotechnik und Informationstechnik*, **8**, 104 (2020).
- M. Singh, J. Kaiser, and H. Hahn, "Thick electrodes for high energy lithium ion batteries." *J. Electrochem. Soc.*, **162**, A1196 (2015).
- J. Sturm, A. Rheinfeld, I. Zilberman, F. B. Spingler, S. Kosch, F. Frie, and A. Jossen, "Modeling and simulation of inhomogeneities in a 18650 nickel-rich, silicon-graphite lithium-ion cell during fast charging." *Journal of Power Sources*, **412**, 204 (2019).
- G. Reinhart, T. Zeilinger, J. Kurfer, M. Westermeier, C. Thiemann, M. Glonegger, M. Wunderer, C. Tammer, M. Schweier, and M. Heinz, "Research and demonstration center for the production of large-area lithium-ion cells." *Future Trends in Production Engineering*, ed. G. Schuh, R. Neugebauer, and E. Uhlmann (Springer, Berlin, Heidelberg) Vol. 12, p. 3 (2013).
- D. Schreiner et al., "Comparative evaluation of lmr-ncm and nca cathode active materials in multilayer lithium-ion pouch cells—part I: production, electrode characterization, and formation." *J. Electrochem. Soc.*, **168**, 030507 (2021).
- T. Teuffl, B. Strehle, P. Müller, H. A. Gasteiger, and M. A. Mendez, "Oxygen release and surface degradation of Li- and Mn-rich layered oxides in variation of the Li₂MnO₃ content." *J. Electrochem. Soc.*, **165**, A2718 (2018).
- A. Guéguen, C. Bolli, M. A. Mendez, and E. J. Berg, "Elucidating the reactivity of tris(trimethylsilyl)phosphite and tris(trimethylsilyl)phosphate additives in carbonate electrolytes—a comparative online electrochemical mass spectrometry study." *ACS Appl. Energy Mater.*, **3**, 290 (2020).
- S.-H. Kang, W.-S. Yoon, K.-W. Nam, X.-Q. Yang, and D. P. Abraham, "Investigating the first-cycle irreversibility of lithium metal oxide cathodes for Li batteries." *J. Mater. Sci.*, **43**, 4701 (2008).
- S. S. Zhang, "Identifying rate limitation and a guide to design of fast-charging Li-ion battery." *InfoMat*, **2**, 942 (2020).
- J. Zheng, W. Shi, M. Gu, J. Xiao, P. Zuo, C. Wang, and J.-G. Zhang, "Electrochemical kinetics and performance of layered composite cathode material Li[Li_{0.2}Ni_{0.2}Mn_{0.6}]O₂." *J. Electrochem. Soc.*, **160**, A2212 (2013).
- W. Mao, G. Ai, Y. Dai, Y. Fu, X. Song, H. Lopez, and V. Battaglia, "Nature of the impedance at low states of charge for high-capacity, lithium and manganese-rich cathode materials." *J. Electrochem. Soc.*, **163**, A3091 (2016).
- P. Meister, H. Jia, J. Li, R. Kloepsch, M. Winter, and T. Placke, "Best practice: performance and cost evaluation of lithium ion battery active materials with special emphasis on energy efficiency." *Chemistry of Materials*, **28**, 7203 (2016).
- J. Wandt, A. T. Freiberg, A. Ogdronik, and H. A. Gasteiger, "Singlet oxygen evolution from layered transition metal oxide cathode materials and its implications for lithium-ion batteries." *Mater. Today*, **21**, 825 (2018).
- K. Kim, I. Park, S.-Y. Ha, Y. Kim, M.-H. Woo, M.-H. Jeong, W. C. Shin, M. Ue, S. Y. Hong, and N.-S. Choi, "Understanding the thermal instability of fluoroethylene carbonate in LiPF₆-based electrolytes for lithium ion batteries." *Electrochimica Acta*, **225**, 358 (2017).
- T. Teuffl, D. Pritzl, P. Krieg, B. Strehle, M. A. Mendez, and H. A. Gasteiger, "Operating EC-based electrolytes with Li- and Mn-rich NCMs: the role of O₂-release on the choice of the cyclic carbonate." *J. Electrochem. Soc.*, **167**, 110505 (2020).
- T. Teuffl, D. Pritzl, S. Solchenbach, M. A. Mendez, and H. A. Gasteiger, (2021), Thermal stability of FEC-based electrolytes for high-voltage Li-ion batteries, Manuscript in preparation.
- M. Uitz, M. Stenad, S. Breuer, C. Täubert, T. Traußnig, V. Hennige, I. Hanzu, and M. Wilkening, "Aging of Tesla's 18650 lithium-ion cells: correlating solid-electrolyte-interphase evolution with fading in capacity and power." *J. Electrochem. Soc.*, **164**, A3503 (2017).
- S. Hildebrand, C. Vollmer, M. Winter, and F. M. Schappacher, "Al₂O₃, SiO₂ and TiO₂ as coatings for Safer LiNi_{0.8}Co_{0.15}Al_{0.05}O₂ cathodes: electrochemical

- performance and thermal analysis by accelerating rate calorimetry." *J. Electrochem. Soc.*, **164**, A2190 (2017).
49. J. Li, J. Harlow, N. Stakheiko, N. Zhang, J. Paulsen, and J. Dahn, "Dependence of cell failure on cut-off voltage ranges and observation of kinetic hindrance in $\text{LiNi}_{0.8}\text{Co}_{0.15}\text{Al}_{0.05}\text{O}_2$." *J. Electrochem. Soc.*, **165**, A2682 (2018).
 50. D. Mohanty, A. S. Sefat, J. Li, R. A. Meisner, A. J. Rondinone, E. A. Payzant, D. P. Abraham, D. L. Wood, and C. Daniel, "Correlating cation ordering and voltage fade in a lithium-manganese-rich lithium-ion battery cathode oxide: a joint magnetic susceptibility and TEM study." *Physical Chemistry Chemical Physics: PCCP*, **15**, 19496 (2013).
 51. D. Mohanty, J. Li, D. P. Abraham, A. Huq, E. A. Payzant, D. L. Wood, and C. Daniel, "Unraveling the voltage-fade mechanism in high-energy-density lithium-ion batteries: origin of the tetrahedral cations for spinel conversion." *Chemistry of Materials*, **26**, 6272 (2014).
 52. M. Sathya et al., "Origin of voltage decay in high-capacity layered oxide electrodes." *Nat. Mater.*, **14**, 230 (2015).
 53. K. Kleiner, B. Strehle, A. R. Baker, S. J. Day, C. C. Tang, I. Buchberger, F.-F. Chesneau, H. A. Gasteiger, and M. Piana, "Origin of high capacity and poor cycling stability of Li-rich layered oxides: a long-duration in situ synchrotron powder diffraction study." *Chemistry of Materials*, **30**, 3656 (2018).
 54. M. Wohlfahrt-Mehrens, C. Vogler, and J. Garche, "Aging mechanisms of lithium cathode materials." *Journal of Power Sources*, **127**, 58 (2004).
 55. J. Vetter, P. Novák, M. R. Wagner, C. Veit, K.-C. Möller, J. O. Besenhard, M. Winter, M. Wohlfahrt-Mehrens, C. Vogler, and A. Hammouche, "Ageing mechanisms in lithium-ion batteries." *Journal of Power Sources*, **147**, 269 (2005).
 56. Y. Wu, P. Keil, S. F. Schuster, and A. Jossen, "Impact of temperature and discharge rate on the aging of a $\text{LiCoO}_2/\text{LiNi}_{0.8}\text{Co}_{0.15}\text{Al}_{0.05}\text{O}_2$ lithium-ion pouch cell." *J. Electrochem. Soc.*, **164**, A1438 (2017).
 57. P. Keil and A. Jossen, "Impact of dynamic driving loads and regenerative braking on the aging of lithium-ion batteries in electric vehicles." *J. Electrochem. Soc.*, **164**, A3081 (2017).
 58. F. Friedrich, B. Strehle, A. T. S. Freiberg, K. Kleiner, S. J. Day, C. Erk, M. Piana, and H. A. Gasteiger, "Choice-capacity fading mechanisms of NCM-811 cathodes in lithium-ion batteries studied by X-ray diffraction and other diagnostics." *J. Electrochem. Soc.*, **166**, A3760 (2019).